CHIN. PHYS. LETT. Vol. 34, No. 6 (2017) 067301

Coulomb-Dominated Oscillations in Fabry–Perot Quantum Hall Interferometers *

Yu-Ying Zhu(朱玉莹)[1,2], Meng-Meng Bai(白孟孟)[1,2], Shu-Yu Zheng(郑树玉)[1], Jie Fan(樊洁)[1], Xiu-Nian Jing(景秀年)[1,3], Zhong-Qing Ji(姬忠庆)[1], Chang-Li Yang(杨昌黎)[1,3], Guang-Tong Liu(刘广同)[1**], Li Lu(吕力)[1,3]

[1] *Beijing National Laboratory for Condensed Matter Physics, Institute of Physics, Chinese Academy of Sciences, Beijing 100190*

[2] *University of Chinese Academy of Sciences, Beijing 100049*

[3] *Collaborative Innovation Center of Quantum Matter, Beijing 100871*

(Received 9 March 2017)

Periodic resistance oscillations in Fabry–Perot quantum Hall interferometers are observed at integer filling factors of the constrictions, $f_c = 1$, 2, 3, 4, 5 and 6. Rather than the Aharonov–Bohm interference, these oscillations are attributed to the Coulomb interactions between interfering edge states and localized states in the central island of an interferometer, as confirmed by the observation of a positive slope for the lines of constant oscillation phase in the image plot of resistance in the B–V_S plane. Similar resistance oscillations are also observed when the area A of the center regime and the backscattering probability of interfering edge states are varied, by changing the side-gate voltages and the configuration of the quantum point contacts, respectively. The oscillation amplitudes decay exponentially with temperature in the range of 40 mK$< T \leq$ 130 mK, with a characteristic temperature $T_0 \sim 25$ mK, consistent with recent theoretical and experimental works.

PACS: 73.43.Jn, 73.23.−b, 73.43.−f DOI: 10.1088/0256-307X/34/6/067301

Under a strong perpendicular magnetic field, a two-dimensional electronic system (2DES) exhibits the quantum Hall effects (QHEs),[1,2] where the bulk of the 2DES is insulating and the electronic transport is dominated by extended edge states located at the sample edge. As a powerful tool to study basic properties of the elementary quasiparticles of a quantum Hall system, the interferometry of edge states has been a subject of considerable interest in the last two decades. In particular, the exotic fractional charge and anyonic statistics of fractional quantum Hall states (FQHS) can be probed by utilizing an electronic Fabry–Perot interferometer,[3−5] which consists of two quantum point contacts (QPCs) fabricated from a 2DES. Recent interest focused on the Fabry–Perot quantum Hall interferometer (FPQHI) has been largely stimulated by its potential to probe the predicted non-Abelian statistics of a 5/2 FQHS[6−12] and the possibility to use such a device as building blocks for topological quantum computation.[13,14]

In an FPQHI, the innermost quantum Hall edge mode of the two QPC constrictions is partially transmitted due to the inter-edge scattering, giving rise to an interference between edge states backscattered at the two constrictions. The interfering edge channel separates two quantum Hall states (QHSs) with filling factors $f_i > f_o$, where f_i (f_o) is the inner (outer) QHS. The relative phase of the interference is a combination of the Aharonov–Bohm (AB) phase and the statistical phase accumulated by one quasiparticle of the f_i QHS propagating along the interfering edge,

$$\theta = 2\pi e_i^* B A_I/\phi_0 + N_L\theta_p, \tag{1}$$

where e_i^* is the elementary charge of the f_i QHS (in units of the electron charge e), B is the magnetic field, A_I is the area enclosed by the interfering loop, $\phi_0 = h/e$ is the flux quanta, N_L is the number of localized quasiparticles inside the loop, and θ_p is the statistical phase by one quasiparticle encircling another. In Eq. (1), $e_i^* = 1$ and $\theta_p = 0$ for integer quantum Hall state (IQHS). For FQHS, e_i^* is fractional and θ_p is the corresponding anyonic phase. In general, the area $A_I = \bar{A} + \delta A$ is as functions of B and the gate voltage V_g, with δA rapidly oscillating with small amplitude around the relatively large and slowly varying base $\bar{A}$. The oscillatory δA contributes rapid oscillation to the interference phase, as given in Eq. (1), for the backscattering probability of the interfering edge state. This leads to oscillatory magnetoresistances measured across the two constrictions of the FPQHI, with magnetic field period $\Delta B \sim \phi_0/\bar{A}$ or gate voltage period ΔV_g on a scale corresponding to $\Delta N_L = 1$.

By the Coulomb interactions, the interfering edge mode is coupled to localized quasiparticles in the bulk of the central island, and the periodicity of the magnetoresistance is closely related to the coupling strength. Modeling the energy of the FPQHI in terms of a capacitor network,[5] Halperin *et al.* found the period of the magnetic field at fixed V_g,

$$\Delta B = \frac{\phi_0}{\bar{A}}\frac{1}{f_i/e_i^* - f_o/e_o^*}, \tag{2}$$

in the limit of negligible bulk-edge coupling, where e_o^* is the elementary charge of the f_o QHS. This is referred to as the AB limit, since $\Delta B = \phi_0/\bar{A}$ is characteristic to the standard AB effect for IQHS ($f_i = f_o+1$, $e_i^* = e_o^* = 1$). On the other hand, in the Coulomb-

*Supported by the National Basic Research Program of China under Grant No 2014CB920904, the National Natural Science Foundation of China under Grant No 91221203, and the Strategic Priority Research Program B of the Chinese Academy of Sciences under Grant No XDB07010200.

**Corresponding author. Email: gtliu@iphy.ac.cn

© 2017 Chinese Physical Society and IOP Publishing Ltd

dominated (CD) limit where the bulk-edge coupling is sufficiently strong,

$$\Delta B = \frac{\phi_0}{\bar{A}} \frac{e_o^*}{f_o}. \tag{3}$$

Equations (2) and (3) show quantitative difference for ΔB at fixed V_g, while the distinction between the AB and CD limits is most prominent in the image plot of resistance in the B–V_g plane, where a series of stripes with negative and positive slope, respectively, are shown as constant phase lines.[5,19] In the mixed regime between the AB and CD limits, the image plot often shows a checkerboard pattern rather than straight stripes.[5]

Experimentally, magnetoresistance oscillations in FPQHI devices have been reported by several groups, in the IQHS regime[15–20] and FQHS regime.[21–28] Most of the observations, on FPQHIs with small areas ($\bar{A} \leq 5\,\mu m^2$), are consistent with the CD interference,[18–20,27,28] while behaviors of AB interference have been clearly observed on FPQHIs with larger areas ($\bar{A} > 15\,\mu m^2$).[19,27]

In this study, we report on our observations of periodic oscillations in electronic FPQHIs. The observed oscillations are of the CD interference in the IQHS regime, with the characteristics: (1) Magnetic field periods follow Eq. (3) as

$$\Delta B = \frac{\phi_0}{A} \frac{1}{f_c}, \tag{4}$$

where A is the effective area of the interferometer's central island, and f_c is the integer filling factor of the QPC constrictions. (2) Periods of side-gate voltage ΔV_S are independent of f_c. (3) A positive slope for the constant phase lines in the 2D image plot of resistance R in the B–V_S plane. Detailed studies on these oscillations were performed by tuning the area of central island and the backscattering probability of edge modes at the constrictions, via the voltages of sidegates and QPCs, respectively. Oscillations at odd integer Hall plateaus $f_c = 3$ and 5, which are usually hard to detect due to smaller energy gaps,[20] were also clearly observed in our experiments. Temperature-dependent data of the oscillation amplitude show the usual relation $\overline{\delta R} \propto exp(-T/T_0)$,[23,28] with a characteristic temperature around $T_0 \sim 25$ mK. These works performed in the integer quantum Hall regime on samples with relative low mobilities, paved the way for our further study in the fractional quantum Hall regime of higher mobility samples.

Interferometer samples were fabricated on 2DES cleaved from GaAs/AlGaAs heterostructure wafers that were grown by our high vacuum molecular beam epitaxy (MBE) machine. A schematic layout of the sample is shown in Fig. 1(a), with the definition of characteristic dimensions. Ohmic contacts were prepared sequentially by the UV photo-lithography, metal deposition (Pd/Ge/Au: 22/55/150 nm), lift-off, and thermal annealing at 450°C in an atmosphere of forming gas. Then the core of the device, consisting of three pairs of front gates, as shown in Fig. 1(b) by a typical AFM image, were fabricated by e-beam lithography with subsequent metal deposition (Ti/Au: 10/60 nm) and lift-off processes.

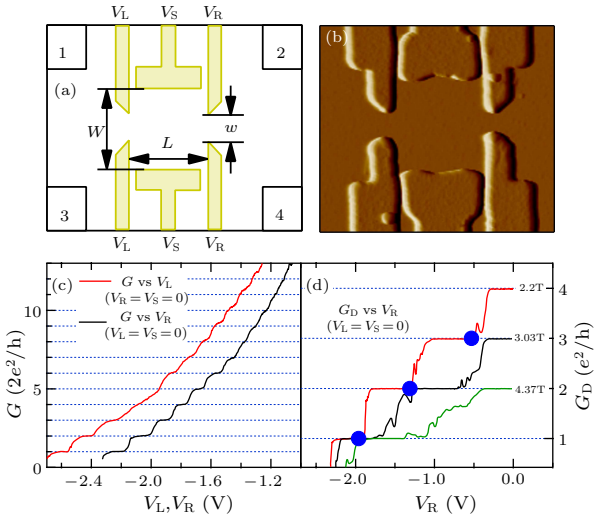

Fig. 1. (a) A schematic layout of the interferometer sample, with the definition of characteristic dimensions. (b) A typical AFM image showing the core of the interferometer, which consists of three pairs of front gates. (c) Quantized conductance plateaus observed on sample S1 at zero magnetic field with sweeping gate voltages V_L and V_R, respectively. (d) Depopulation of edge state modes of the right QPC by its gate voltage V_R, observed on S1 at fixed magnetic fields $B = 2.20$ T, 3.03 T, and 4.37 T, in which the blue solid dots, on the trace of $B = 2.20$ T, mark the points where the edge modes with index $i = 3$, 2, and 1 are just becoming the innermost, respectively.

Table 1. Parameters of the interferometer samples.

Sample	Wafer	L (μm)	W (μm)	w (nm)	$L \times W$ (μm^2)
S1	QW	1.3	1.5	440	1.95
S2	QW	1.3	1.5	440	1.95
S3	QW	1.3	2	440	2.6
S4	HS	1.5	2.2	440	3.3

The interferometer is defined and controlled by applying dc voltages onto the front gates. In our experiments, the same voltage was applied to both gates of each pair, and the voltages on the left QPC, sidegate, and right QPC are denoted by V_L, V_S, and V_R, respectively. Transport measurements were performed in a top-loading dilution refrigerator with a base temperature of 15 mK and a 18-Tesla superconducting magnet. The resistances, $R_D = (V_1 - V_4)/I_{3\to2}$ and $R_L = (V_3 - V_4)/I_{1\to2}$, were measured employing a standard low-frequency (30.9 Hz) lock-in technique, with an excitation current of 1 nA (except 0.5 nA for the variable temperature measurements). Data from four samples, labeled S1, S2, S3, and S4, are presented in this work. The characteristic parameters of these samples are listed in Table 1.

For a QPC, quantized conductance plateaus appear due to depopulation of 1D subbands by sweeping the gate voltage. At zero magnetic field, the conductance plateaus occur whenever $M = 2w/\lambda_F$ is an integer, where w is the effective width of the narrow constriction of the QPC, and λ_F is the Fermi wavelength of the nearby electrons. The conductance of

the plateau is given by[29]

$$G = I_{1\to2}/(V_3 - V_4) = M \cdot 2e^2/h. \quad (5)$$

As shown in Fig. 1(c), the quantized conductance plateaus of a single QPC are clearly observed for sample S1 at zero magnetic field $B = 0$. The conductance curves against gate voltage do not overlap between the left QPC and the right QPC, indicating that their actual widths are different after fabrication despite their designs being symmetrical. According to Eq. (5), the tunability of the gate voltage on the width of the QPC, $\alpha \equiv \partial w/\partial V_g \sim 240\,\text{nm/V}$, can be roughly estimated from the slope of G against gate voltage.

On the other hand, at high magnetic fields, the conductance plateaus occur whenever the Landau level filling factor of the constriction, f_c, is an integer, giving a quantized conductance

$$G_D \equiv 1/R_D = I_{3\to2}/(V_1 - V_4) = f_c \cdot e^2/h. \quad (6)$$

Deviation from the conductance plateau is due to partial reflection of the innermost edge mode via inter-edge scattering that is tunable by the gate voltage. With sweeping the gate voltage toward the negative direction, the new conductance plateau starts at the point where the present innermost edge mode becomes totally reflected and the next inner mode just becomes the innermost. Therefore, the distance in real space between neighboring edge states can be estimated from the voltage spacing between adjacent starting points of the conductance plateaus. For example, Fig. 1(d) shows that at $B = 2.2\,\text{T}$ the right QPC of S1 has four edge modes around zero gate voltage, which can be indexed by $i = 1, 2, 3$ and 4 from the edge to the inner. The three blue dots that mark the starting point of the new conductance plateaus correspond to the respective points where the $i = 3$, 2 and 1 edge modes are just becoming the innermost, respectively. From the voltage spacing of neighboring blue dots, $\Delta V_R \sim 0.6\,\text{V}$, we can estimate a change of the QPC width $\delta w = \alpha \Delta V_R \sim 140\,\text{nm}$, and the distances between the neighboring edge modes, $d_{4,3}$ and $d_{3,2}$, are roughly $\delta w/2 \sim 70\,\text{nm} \sim 4l_B$, where $l_B = \sqrt{\hbar/eB}$ is the magnetic length.

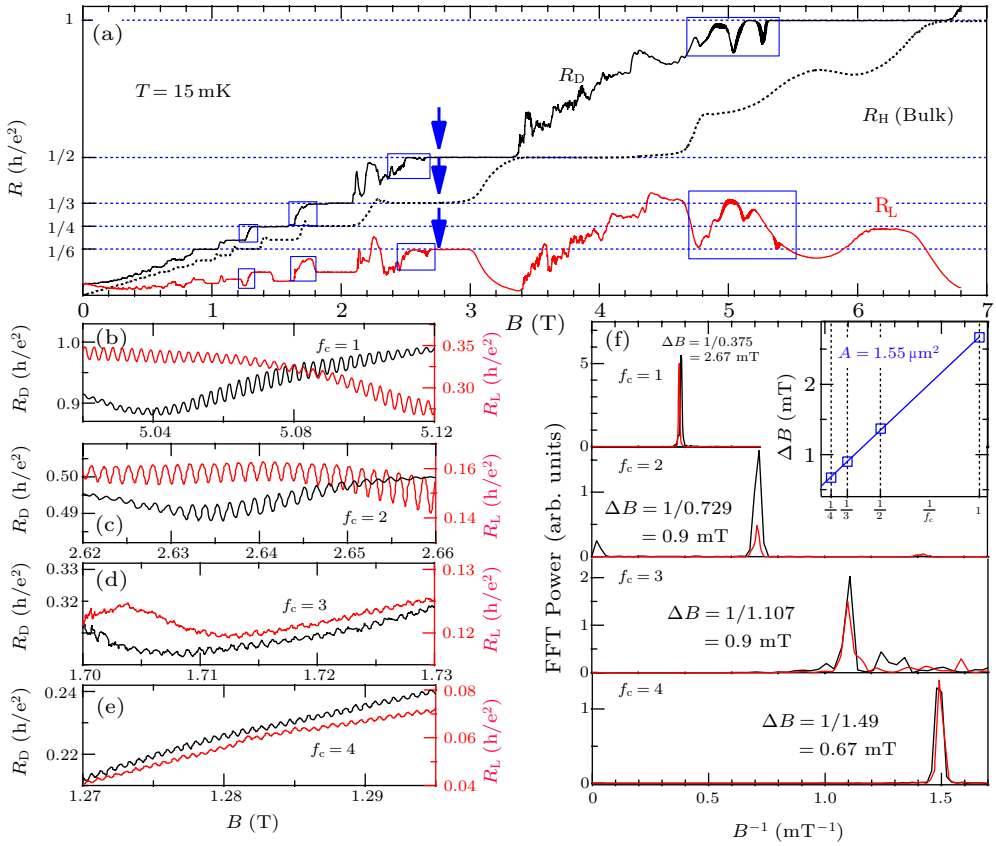

Fig. 2. Transport data measured on sample S2 at $T = 15\,\text{mK}$. (a) Diagonal resistance R_D and longitudinal resistance R_L as a function of perpendicular magnetic field B, measured at $V_L = -0.8\,\text{V}$, $V_R = -0.6\,\text{V}$, and $V_S = -0.6\,\text{V}$; R_H is the R_D trace measured with all gates grounded, representing the Hall resistance of the electrons in the bulk region of the device. (b)–(e) Expanded views of the data in Fig. 2(a), showing periodic oscillations at $f_c = 1$, 2, 3 and 4, respectively. (f) Fast Fourier transform analyses on the sets of oscillations in (b)–(e). Inset: plot of the oscillation periods, ΔB, against $1/f_c$, which exhibits a linear relationship that is characteristic of the CD oscillations of the interferometer, with an area $A \approx 1.55\,\mu\text{m}^2$.

The dependencies of R_D and R_L on magnetic field B are shown in Fig. 2(a) for sample S2. The gate voltages of the QPCs, R_L and V_R, were respectively set at $-0.8\,\text{V}$ and $-0.6\,\text{V}$, such that the two constrictions had the same electron density, $n_c \approx 0.75 n_b$, where n_c and n_b are the electron densities of the constrictions and bulk, respectively. Within the Landauer–Buttiker formalism, the electron transport of the interferometer

is given by[26]

$$R_{\rm L} = \left(\frac{1}{f_{\rm c}} - \frac{1}{f_{\rm b}}\right) \cdot \frac{h}{e^2}, \tag{7}$$

$$R_{\rm D} = \frac{1}{f_{\rm c}} \cdot \frac{h}{e^2}, \tag{8}$$

where $f_{\rm b}$ is the Landau level filling factor in the bulk region.

As an example, the blue arrows in Fig. 2(a) mark the regime where both the constrictions and the bulk are quantized, at $f_{\rm c} = 2$ and $f_{\rm b} = 3$, respectively, as evidenced by the plateaus of $R_{\rm D}$ and $R_{\rm H}$ traces. In this regime, according to Eq. (7), $R_{\rm L}$ should also be quantized giving rise to a plateau at $R_{\rm L} = 6h/e^2$, which has been confirmed by the measured $R_{\rm L}$ trace.

In Fig. 2(a), the most significant observation on the $R_{\rm D}$ and $R_{\rm L}$ traces is the occurrence of periodic oscillations on the low field side of the plateaus of $f_{\rm c} = 1$, 2, 3 and 4. For $f_{\rm c} = 1$ and 2, more than 150 oscillation peaks can be resolved, with amplitudes of the order $0.05e^2/h$. Expanded views of the data in Fig. 2(a) are shown in Figs. 2(b)–2(e), for the oscillations occurring at $f_{\rm c} = 1$, 2, 3 and 4, respectively. Fast Fourier transform (FFT) analyses, as shown in Fig. 2(f), reveal a sharp peak of a single frequency for each set of oscillations, indicating their good periodicity. The oscillation periods, ΔB, obtained from the FFT analyses and plotted in the inset of Fig. 2(f), exhibit a linear dependence on $1/f_{\rm c}$ that is characteristic of the CD oscillations of the interferometer. According to Eq. (4), the effective area $\bar{A}$ of the central island of the interferometer can be determined from the slope of ΔB against $1/f_{\rm c}$. As shown in the inset of Fig. 2(f), $A \approx 1.55\,\mu{\rm m}^2$ is obtained for S2 at $V_{\rm S} = -0.6\,{\rm V}$, which is smaller but reasonably close to the value ($1.95\mu{\rm m}^2$) of its e-beam lithography design.

The magneto-resistance oscillations were also studied on different samples with different central areas. In general, a linear relationship between ΔB and $1/f_{\rm c}$ is found, as shown in Fig. 3(a). Moreover, Fig. 3(b) shows the color map of $R_{\rm D}$ in the plane of B and $V_{\rm S}$, measured on S1 at $f_{\rm c} = 1$ and 2, respectively, with the gate voltages $V_{\rm L} = -1.2\,{\rm V}$, $V_{\rm R} = -1.0\,{\rm V}$ and $V_{\rm S} = -0.7\,{\rm V}$. Obviously, for $f_{\rm c} = 1$ and 2, the oscillation stripes have a positive slope and similar gate voltage periods $\Delta V_{\rm S} \approx 4.4\,{\rm mV}$, confirming their CD origin. Note that the data for the color maps were taken with a constant voltage on one of the side-gates while the other was slowly varied.

The oscillations were observed on the sample S2 at various side-gate voltage $V_{\rm S}$. Figure 3(c) shows the corresponding area A (determined from measured period ΔB) and $\Delta V_{\rm S}$ measured at $f_{\rm c} = 1$, plotted against $V_{\rm S}$. For integer $f_{\rm c}$, due to charge balancing in the central island of the interferometer, the period of side-gate voltage $\Delta V_{\rm S}$ is given by[5,28]

$$\Delta V_{\rm S} = \frac{1}{dA/dV_{\rm S}} \cdot \frac{\phi_0}{(n_{\rm b}\phi_0 - Bf_{\rm c})}. \tag{9}$$

For S2, $dA/dV_{\rm S}$ and $n_{\rm b}\phi_0$ can be estimated from the slope of A versus $V_{\rm S}$ in Fig. 3(c) and from the $R_{\rm H}$ trace of Fig. 2(a), respectively, resulting in $dA/dV_{\rm S} \sim 0.53\,\mu{\rm m}^2/{\rm V}$ and $n_{\rm b}\phi_0 \approx 8.0\,{\rm T}$. With these estimates, $\Delta V_{\rm S}$ can be calculated from Eq. (9), using the actual $Bf_{\rm c}$ value corresponding to each data point of the experimental $\Delta V_{\rm S}$ versus $V_{\rm S}$ plot; the results are shown in Fig. 3(c) as green circles, in reasonable agreement with the experimental points, denoted by red solid circles.

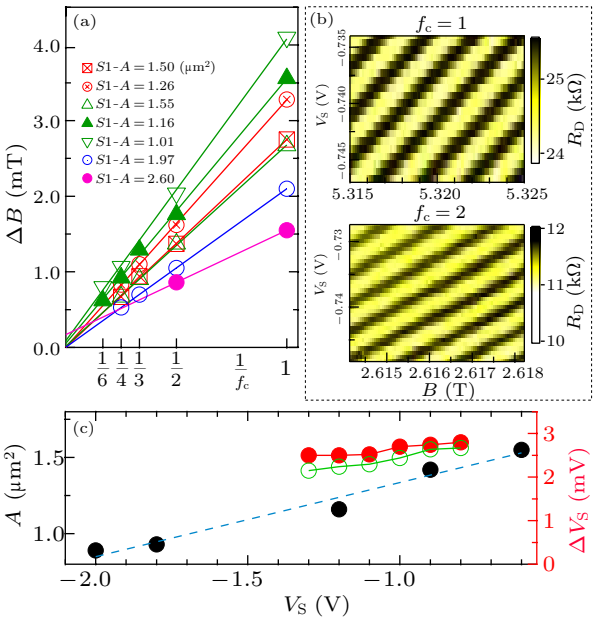

Fig. 3. (a) The value of ΔB versus $1/f_{\rm c}$ for different samples and areas, (b) $R_{\rm D}$ as a color map in the plane of B and $V_{\rm S}$, for $f_{\rm c} = 1$ and 2, respectively, and (c) $V_{\rm S}$ dependence of the central island area A (left axis) and period $\Delta V_{\rm S}$ (right axis). Here the green circles are $\Delta V_{\rm S}$ calculated from Eq. (9).

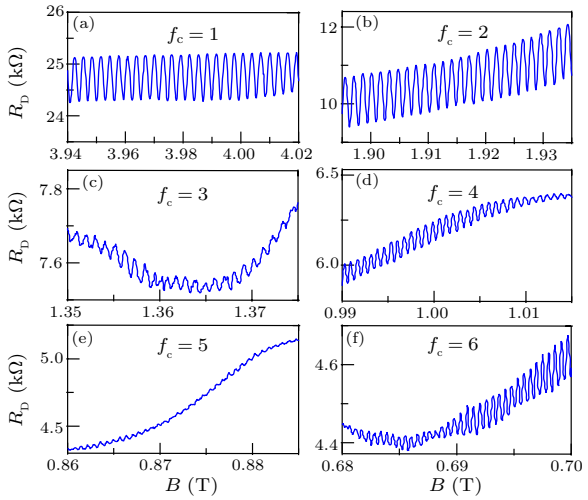

Fig. 4. Stronger oscillations than that of Fig. 2, measured at $T = 15\,{\rm mK}$ on the same sample S2 with different gate voltages ($V_{\rm L} = -1.3\,{\rm V}$, $V_{\rm R} = -1.0\,{\rm V}$, and $V_{\rm S} = -0.7\,{\rm V}$). (a)–(f) Periodic magnetoresistance oscillations observed at $f_{\rm c} = 1$, 2, 3, 4, 5 and 6, respectively.

We have tuned the backscattering probability of the constrictions by varying the QPC gate voltages. Figure 4 shows oscillations measured on S2 with $V_{\rm L} = -1.3\,{\rm V}$, $V_{\rm R} = -1\,{\rm V}$, and $V_{\rm S} = -0.7\,{\rm V}$, which sat-

isfy $n_c \approx 0.6n_b$. Now the oscillations are stronger than those shown in Fig. 2 for the same sample with $V_L = -0.8$ V and $V_R = -0.6$ V; the oscillations are observed at $f_c = 6$, and even at $f_c = 5$, where observation on similar oscillations has hardly been reported.

Figure 5 displays the temperature evolution of magnetoresistance oscillations δR_D measured on sample S3 (δR_D with its smooth background subtracted) in the 10 mK$\leq T \leq$ 130 mK temperature range. The oscillation amplitude $\overline{\delta R}$, averaged over $\sim$ 10 periods in the zone enclosed by the blue frame in Fig. 5, is plotted in the inset of Fig. 5. The relation $\overline{\delta R} \propto \exp(-T/T_0)$ is found, in the regime of $T \geq 40$ mK, in agreement with recent theoretical predictions[5] and experimental results.[23,28] The characteristic temperature $T_0 = 23.8$ mK is extracted by fitting this curve. At $T \leq 40$ mK, the oscillation amplitude tends to saturate, possibly due to unintentional electron heating by the environment of the measurement setup.

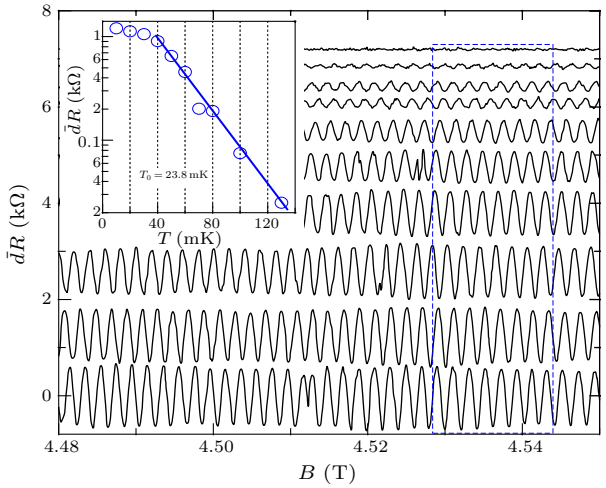

Fig. 5. Temperature dependence of the oscillations measured on S3 at $f_c = 1$ ($V_L = V_R = V_S = -0.8$ V). The curves are shifted vertically for clarity. Inset: the oscillation amplitude, $\overline{\delta R}$, averaged over $\sim$ 10 periods in the zone enclosed by the blue frame, versus temperature T; curve fitting to $\overline{\delta R} \propto \exp(-T/T_0)$ yields a characteristic temperature $T_0 = 23.8$ mK.

In summary, we have observed the Coulomb-dominated magnetoresistance oscillations at various integer quantum Hall states ($f_c = 1$, 2, 3, 4, 5 and 6) in the Fabry–Perot quantum Hall interferometers. These oscillations have been studied by tuning the area of the central island and the backscattering probability of edge modes at the constrictions, by varying the voltages of sidegates and QPCs, respectively. Although usually hard to detect due to smaller energy gaps, oscillations at odd integer Hall plateaus $f_c = 3$ and 5 are also clearly observed in our experiments. Temperature dependence data of the oscillation amplitude show the usual relationship $\overline{\delta R} \propto \exp(-T/T_0)$, with the characteristic temperature around $T_0 \sim 25$ mK. These works, performed in the integer quantum Hall regime on samples with relatively low mobilities, have paved the way for our future study on the observation of CD and AB oscillations in the fractional quantum Hall regime of samples with higher mobility.

We acknowledge helpful discussions with Wan X, Hu Z X and Du R R.

References

[1] Das Sarma S and Pinczuk A 1997 *Perspectives in Quantum Hall Effect* (New York: Wiley and Sons)
[2] Ezawa Z F 2008 *Quantum Hall Effects: Field Theoretical Approach and Related Topics* 2nd edn (Singapore: World Scientific)
[3] Chamon C de C, Freed D E, Kivelson S A, Sondhi S L and Wen X G 1997 *Phys. Rev.* B **55** 2331
[4] Rosenow B and Halperin B I 2007 *Phys. Rev. Lett.* **98** 106801
[5] Halperin B I, Stern A, Neder I and Rosenow B 2011 *Phys. Rev.* B **83** 155440
[6] Willett R, Eisenstein J P, Stormer H L, Tsui D C, Gossard A C and English J H 1987 *Phys. Rev. Lett.* **59** 1776
[7] Pan W, -S J, Shvarts V, Adams D E, Stormer H L, Tsui D C, Pfeiffer L N, Baldwin K W and West K W 1999 *Phys. Rev. Lett.* **83** 3530
[8] Moore G and Read N 1992 *Nucl. Phys.* B **374** 615
[9] Read N and Rezayi E 1996 *Phys. Rev.* B **54** 16864
[10] Wen X G 1991 *Phys. Rev. Lett.* **66** 802
[11] Bonderson P, Kitaev A and Shtengel K 2006 *Phys. Rev. Lett.* **96** 016803
[12] Stern A and Halperin B I 2006 *Phys. Rev. Lett.* **96** 016802
[13] Sarma S D, Freedman M and Nayak C 2005 *Phys. Rev. Lett.* **94** 166802
[14] Nayak C, Simon S H, Stern A, Freedman M and Sarma S D 2008 *Rev. Mod. Phys.* **80** 1083
[15] van Wees B J, Kouwenhoven L P, Harmans C J P M, Williamson J G, Timmering C E, Broekaart M E I, Foxon C T and Harris J J 1989 *Phys. Rev. Lett.* **62** 2523
[16] Bird J P, Ishibashi K, Stopa M, Aoyagi Y and Sugano T 1994 *Phys. Rev.* B **50** 14983
[17] Camino F E, Zhou W and Goldman V J 2005 *Phys. Rev.* B **72** 155313
[18] Camino F E, Zhou Wei and Goldman V J 2007 *Phys. Rev.* B **76** 155305
[19] Zhang Yiming, McClure D T, Levenson-Falk E M, Marcus C M, Pfeiffer L N and West K W 2009 *Phys. Rev.* B **79** 241304(R)
[20] Choi H, Jiang P, Godfrey M D, Kang W, Simon S H, Pfeiffer L N, West K W and Baldwin K W 2011 *New J. Phys.* **13** 055007
[21] Camino F E, Zhou Wei and Goldman V J 2005 *Phys. Rev. Lett.* **95** 246802
[22] Camino F E, Zhou Wei and Goldman V J 2005 *Phys. Rev.* B **72** 075342
[23] Camino F E, Zhou Wei and Goldman V J 2006 *Phys. Rev.* B **74** 115301
[24] Camino F E, Zhou Wei and Goldman V J 2007 *Phys. Rev. Lett.* **98** 076805
[25] Willett R L, Pfeiffer L N and West K W 2009 *Proc. Natl. Acad. Sci. USA* **106** 853
[26] Willett R L, Pfeiffer L N and West K W 2010 *Phys. Rev.* B **82** 205301
[27] Ofek N, Bid A, Heiblum M, Stern A, Umansky V and Mahalu D 2010 *Proc. Natl. Acad. Sci. USA* **107** 5276
[28] McClure D T, Chang W, Marcus C M, Pfeiffer L N and West K W 2012 *Phys. Rev. Lett.* **108** 256804
[29] van Wees B J, van Houten H, Beenakker C W J, Williamson J G, Kouwenhoven L P, van der Marel D and Foxon C T 1988 *Phys. Rev. Lett.* **60** 848
[30] Davies H 1988 *The Physics of Low-Dimensional Semiconductors* (Cambridge: Cambridge University)